

Elliptical Lens Model in PG 1115+080

Katsuaki ASANO and Takeshi FUKUYAMA

Department of Physics, Ritsumeikan University, Kusatsu, Shiga 525-8577

E-mail(KA): sph10001@bkc.ritsumei.ac.jp

(Received ; accepted)

Abstract

The mass distribution of the lensing galaxy of the multiple quasar PG1115+080 has been studied. Using the observational data of Christian et al. (1987, ApJ 464, 92), we applied a single elliptical lens model with a softened power-law behavior. It has been revealed that the image positions, amplifications and time delays of this lensing system cannot be explained by the single transparent lens model. We compare this elliptical lens model with a multipole expansion model.

Key words: Gravitational lenses—Galaxies: structure—Quasars: individual(PG 1115+080)

1. Introduction

We discuss the multiple quasar PG 1115+080 using an elliptical lens model with a softend power-law behavior.

The same theme was discussed by Narasimha et al. (1982). The motivation to repeat this research was as follows. Firstly, they used the observational data by Young et al. (1981). However, the more recent data by Christian et al. (1987) have been adopted by the references Yoshida and Omote (1988), Kakigi et al. (1995). Our purpose, however, was not simply to reanalyze the same object using the new observational data, but to discuss gravitational lensing from many-sided view points. Let us explain its physical meaning more concretely. In gravitational lensing, “the number of degrees of freedom” (\equiv number of fitted observed data— number of fitting parameters, which we call DOF hereafter) is small and it is dangerous to deduce any conclusion by simply having reproduced, for instance, image positions. Indeed, many qualitatively different models can reproduce the restricted observed data. However, this view point has so far gone unnoticed, and usually a numerically tractable simple model has been applied to the respective lensing phenomenon. It is necessary for us to apply various lensing models systematically to the same lensing phenomenon and to compare their results with each other. Together with these numerical approaches, analytical surveys of lensing models are also needed for obtaining a systematic understanding of lensing phenomena.

In this paper, along this line of thought, we systematically formulate an elliptical mass distribution model with various softened power-law behavior. We then apply them to the multiple quasar PG 1115+080. The results are compared with those obtained by a qualitatively different model, a multipole expansion model.

This lensing galaxy is relatively isolated in comparison with other lensing events, and has quadruple images of the background quasars (Young et al. 1981; Christian et al. 1987; Kristian et al. 1993). Therefore, this system may be suitable for applying an analytical treatment of the lens models developed in this paper. However, the physical parameters of the lensing object are found to be sensitive to the observed image positions, and especially to the lens position which have been measured with some statistical treatments. In order to obtain reliable pictures of the lensing object we need a variety of more precise data of images. They are the image shape and the precise spectroscopies of every image component and their time variations etc. Together with these improvements of fitted data, it is also necessary to apply qualitatively different models to the same lensing object. For instance, although the elliptical lens model is transparent, the multipole expansion model (Kakigi et al. 1995; Fukuyama et al. 1997) is non-transparent. They give various and even inconsistent aspects of the lensing object. However, from such an

variety of aspects, we expect that the true features of the lensing object will be uncovered. This article is a step towards this goal.

The present paper is organized as follows. We give a general formulation of the elliptical lens model with a softened power-law behavior in section 2. The case for $k \leq 3$ (power of distance dependence on the lensing mass density) is discussed in detail. In section 3, the given formulation is applied to the PG 1115+080 lensing system. The best-fit parameters for $k = 2$ and $k = 3$ are given. These parameters give the aspect of a lensing object that is qualitatively different from that of Narasimha et al. This mainly comes from the fact that the lens position assumed by Narashimha et al. is different from ours, which is fixed with the observed position by Christian et al. In section 4, we argue about the discrepancies of our results with the observations and compare the elliptical lens model with the multipole expansion model. Very recently, lens models of PG 1115+080 accompanying the group galaxies have been applied by Keeton and Kochanek (1997) and Schechter et al. (1997). We make some comments concerning them in relation to our article.

2. Formulation

Our lens model is described based on the mass density of Bourassa et al. (1973) (see also Bourassa, Kantowski 1975; Schramm 1990; Kormann et al. 1994; Kassiola, Kovner 1993),

$$\rho(a) = \begin{cases} \rho_0 \left\{ 1 + \left(\frac{a}{r_c} \right)^2 \right\}^{-\frac{k}{2}}, & \text{for } a \leq nr_c \\ 0, & \text{for } a > nr_c \end{cases} \quad (1)$$

with

$$x'^2 + y'^2 + \frac{z'^2}{1-e^2} \equiv a^2. \quad (2)$$

Here, r_c is the core radius and ρ_0 is the constant central density; e is the eccentricity.

We choose the direction of the line-of-sight on the z -axis, which is tilted relative to the symmetry axis z' by angle γ . The situation is depicted by figure 1.

Figure1

Although ϕ is a rotation angle between the x-axis and the major axis of the lens object, in this section we assume $\phi = 0$. The principal coordinates of a spheroid (x', y', z') are related with (x, y, z) by

$$\begin{pmatrix} x' \\ y' \\ z' \end{pmatrix} = \begin{pmatrix} 1 & 0 & 0 \\ 0 & \cos \gamma & -\sin \gamma \\ 0 & \sin \gamma & \cos \gamma \end{pmatrix} \begin{pmatrix} x \\ y \\ z \end{pmatrix}. \quad (3)$$

Substituting equation (3) into equation (2), we obtain

$$a^2 = b^2 + \frac{1 - e^2 \sin^2 \gamma}{1 - e^2} \left(z + \frac{e^2 y \cos \gamma \sin \gamma}{1 - e^2 \sin^2 \gamma} \right)^2, \quad (4)$$

where

$$b^2 \equiv x^2 + \frac{y^2}{1 - e^2 \sin^2 \gamma}. \quad (5)$$

The surface mass density, $\Sigma(x, y) \equiv \int dz \rho(a)$, is given by

$$\Sigma(x, y) = \sqrt{\frac{1 - e^2}{1 - e^2 \sin^2 \gamma}} \int_{b^2}^{(nr_c)^2} da^2 \frac{\rho(a)}{\sqrt{a^2 - b^2}} \equiv \sqrt{\frac{1 - e^2}{1 - e^2 \sin^2 \gamma}} K_k. \quad (6)$$

Here, K_k have the following forms, depending on the parameter k :

$$K_1 = 2\rho_0 r_c \ln \frac{\sqrt{n^2 + 1} + \sqrt{n^2 - (\frac{b}{r_c})^2}}{\sqrt{1 + \left(\frac{b}{r_c}\right)^2}}, \quad (7)$$

$$K_2 = \frac{2\rho_0 r_c}{\sqrt{1 + (\frac{b}{r_c})^2}} \tan^{-1} \frac{\sqrt{n^2 - (\frac{b}{r_c})^2}}{\sqrt{1 + (\frac{b}{r_c})^2}}, \quad (8)$$

$$K_3 = \frac{2\rho_0 r_c}{1 + (\frac{b}{r_c})^2} \frac{\sqrt{n^2 - (\frac{b}{r_c})^2}}{\sqrt{n^2 + 1}}, \quad (9)$$

$$K_5 = \frac{2\rho_0 r_c}{(1 + (\frac{b}{r_c})^2)^2} \frac{\sqrt{n^2 - (\frac{b}{r_c})^2}}{3(n^2 + 1)^{3/2}} (3 + 2n^2 + (\frac{b}{r_c})^2). \quad (10)$$

Fermat's potential is given by

$$\phi(\mathbf{x}, \mathbf{x}_s) = \frac{1}{2}(\mathbf{x} - \mathbf{x}_s)^2 - \frac{1}{\pi} \int dx' dy' \kappa(\mathbf{x}') \ln |\mathbf{x} - \mathbf{x}_s|. \quad (11)$$

Here, \mathbf{x} and \mathbf{x}_s are the two-dimensional image and source position, respectively. Also, κ is the surface mass density of the lens object,

$$\kappa(\mathbf{x}) = \frac{\Sigma(\mathbf{x})}{\Sigma_{\text{crit}}}, \quad (12)$$

normalized by

$$\Sigma_{\text{crit}} \equiv \frac{c^2 D_s}{4\pi G D_l D_{ls}} (\equiv \frac{c^2}{4\pi G D}). \quad (13)$$

Notations are depicted in figure 2.

Figure2

The lens equation is

$$\mathbf{x}_s = \mathbf{x} - \frac{1}{\pi} \int dx' dy' \kappa(\mathbf{x}') \frac{\mathbf{x} - \mathbf{x}'}{(\mathbf{x} - \mathbf{x}')^2}. \quad (14)$$

In complex notation it becomes

$$z_s = z - \frac{4GD}{c^2} I^*(z), \quad (15)$$

where $z_s \equiv x_s + iy_s$ and $z \equiv x + iy$ (here and hereafter we use the letter z in this sense). $I^*(z)$ is the complex conjugate of $I(z)$, which is defined by

$$I \equiv \int dx' dy' \Sigma(b') \frac{1}{z - z'}. \quad (16)$$

Taking

$$x' = b' \cos \varphi', \quad y' = b' \sqrt{1 - e^2 \sin^2 \gamma} \sin \varphi' \quad (17)$$

into consideration, I is transformed to

$$I = \sqrt{1 - e^2 \sin^2 \gamma} \int_0^{nr_c} db' b' \Sigma(b') \oint d\varphi' \frac{1}{z - b'(\cos \varphi' + i\sqrt{1 - e^2 \sin^2 \gamma} \sin \varphi')}. \quad (18)$$

Here,

$$\oint d\varphi' \frac{1}{z - b'(\cos \varphi' + i\sqrt{1 - e^2 \sin^2 \gamma} \sin \varphi')} = \begin{cases} \frac{\sqrt{z^2}}{z} \frac{2\pi}{\sqrt{z^2 - b'^2 e^2 \sin^2 \gamma}}, & \text{for } b'^2 \leq b^2 = x^2 + \frac{y^2}{1 - e^2 \sin^2 \gamma} \\ 0, & \text{for } b'^2 > b^2. \end{cases} \quad (19)$$

We then obtain

$$I_k = 2\pi \frac{\sqrt{z^2}}{z} \sqrt{1 - e^2 \sin^2 \gamma} \int_0^{\min(nr_c, b)} db' \frac{b' \Sigma_k(b')}{\sqrt{z^2 - b'^2 e^2 \sin^2 \gamma}}. \quad (20)$$

We consider the $k = 2, 3$ cases of mass density, the motivation of which is as follows. The observed brightness distribution of galaxies decays as r^{-3} (Binney, Tremaine 1987). The mass-to-light ratio suggests that the mass distribution decays more mildly than that.

For $k = 3$, I_3 takes the following form:

$$I_3 = \frac{2\pi\rho_0 r_c^2}{\sqrt{n^2 + 1}} \frac{\sqrt{z^2}}{z} \frac{\sqrt{1 - e^2}}{e \sin \gamma} \int_0^{\min(n^2, (\frac{b}{r_c})^2)} \frac{d\omega}{1 + \omega} \sqrt{\frac{\omega - n^2}{w - (\frac{z}{r_c e \sin \gamma})^2}}. \quad (21)$$

Here, we consider the following indefinite integral:

$$\begin{aligned} F &\equiv \int \frac{d\omega}{1 + \omega} \sqrt{\frac{\omega - \beta}{\omega - \alpha}}, \quad \alpha \in \mathbf{C}, \beta \in \mathbf{R} \\ &= \sqrt{\frac{1 + \beta}{1 + \alpha}} \ln \frac{\sqrt{(1 + \alpha)(\omega - \beta)} - \sqrt{(1 + \beta)(\omega - \alpha)}}{\sqrt{(1 + \alpha)(\omega - \beta)} + \sqrt{(1 + \beta)(\omega - \alpha)}} \\ &\quad - \ln \frac{\sqrt{\omega - \beta} - \sqrt{\omega - \alpha}}{\sqrt{\omega - \beta} + \sqrt{\omega - \alpha}}. \end{aligned} \quad (22)$$

Thus, if the images are positioned inside of the cut-off radius nr_c ,

$$\begin{aligned} I_3 &= 2\pi\rho_0 r_c \frac{\sqrt{z^2}}{z} \frac{\sqrt{1 - e^2}}{e \sin \gamma} \left[\frac{1}{\sqrt{n^2 + 1}} \ln \frac{(z_0 - ne \sin \gamma)(A_0 + \sqrt{n^2 - B_0^2})}{(z_0 + ne \sin \gamma)(A_0 - \sqrt{n^2 - B_0^2})} \right. \\ &\quad + \frac{e \sin \gamma}{\sqrt{z_0^2 + e^2 \sin^2 \gamma}} \left\{ \ln \frac{z_0 \sqrt{n^2 + 1} + n \sqrt{z_0^2 + e^2 \sin^2 \gamma}}{z_0 \sqrt{n^2 + 1} - n \sqrt{z_0^2 + e^2 \sin^2 \gamma}} \right. \\ &\quad \left. \left. - \ln \frac{\sqrt{n^2 + 1} A_0 e \sin \gamma + \sqrt{(z_0^2 + e^2 \sin^2 \gamma)(n^2 - B_0^2)}}{\sqrt{n^2 + 1} A_0 e \sin \gamma - \sqrt{(z_0^2 + e^2 \sin^2 \gamma)(n^2 - B_0^2)}} \right\} \right], \end{aligned} \quad (23)$$

where

$$A_0 \equiv \frac{\sqrt{1 - e^2 \sin^2 \gamma}}{er_c \sin \gamma} \left(x + \frac{iy}{1 - e^2 \sin^2 \gamma} \right), \quad B_0 \equiv \frac{b}{r_c} \quad (24)$$

and

$$z_0 \equiv \frac{z}{r_c}. \quad (25)$$

However, if the images are located outside of the cut-off radius, I_3 takes the following form:

$$\begin{aligned} I_3 &= 2\pi\rho_0 r_c \frac{\sqrt{z^2}}{z} \frac{\sqrt{1 - e^2}}{e \sin \gamma} \left[\frac{1}{\sqrt{n^2 + 1}} \ln \frac{(z_0 - ne \sin \gamma)}{(z_0 + ne \sin \gamma)} \right. \\ &\quad \left. + \frac{e \sin \gamma}{\sqrt{z_0^2 + e^2 \sin^2 \gamma}} \ln \frac{z_0 \sqrt{n^2 + 1} + n \sqrt{z_0^2 + e^2 \sin^2 \gamma}}{z_0 \sqrt{n^2 + 1} - n \sqrt{z_0^2 + e^2 \sin^2 \gamma}} \right]. \end{aligned} \quad (26)$$

In the case of $k = 2$, from equations (8) and (20) it follows that

$$I_2 = 2\pi\rho_0 r_c^2 \sqrt{1 - e^2} \frac{\sqrt{z^2}}{z} \int_0^{\min(n^2, B_0^2)} d\omega \frac{1}{\sqrt{1 + \omega}} \tan^{-1} \sqrt{\frac{n^2 - \omega}{1 + \omega}} \cdot \frac{1}{\sqrt{z_0^2 - \omega^2 e^2 \sin^2 \gamma}}. \quad (27)$$

Equation (27) can not be solved analytically, except for $n = \infty$. As for $k = 2$, there is a more conventional model which is used to fit the X-ray surface brightness profile (Miralda-Escudé 1993):

$$\kappa(\theta, \phi) = \begin{cases} \frac{b_0}{2\sqrt{\theta^2(1-\epsilon \cos 2\phi) + r_c^2}}, & \text{for } \theta \leq \theta_{\text{cut}} \\ 0, & \text{for } \theta > \theta_{\text{cut}}. \end{cases} \quad (28)$$

Here, $b_0 = 2\pi\rho_0 r_c^2$, and ϵ is the ellipticity related to the eccentricity by

$$\epsilon = \frac{e^2}{2 - e^2}. \quad (29)$$

As can be easily understood from equations (6) and (8), this corresponds to the $n \rightarrow \infty$ limit in equations (6),(8) with $\gamma = \pi/2$. The length scale in equation (28) is $1/\sqrt{1-\epsilon}$ times longer than that in equation (27). A cut-off of mass distribution is introduced at the level of the surface mass density. Equation (27) seems to be physically more general than equation (28), because equation (28) has no cut-off radius and we can use equation (27) with $\gamma \neq \pi/2$.

We thus consider equation (27). In order to calculate equation (27), we expand it with respect to $e^2 \sin^2 \gamma$. Using

$$\frac{1}{\sqrt{z_0^2 - \omega e^2 \sin^2 \gamma}} \simeq \frac{1}{z_0} + \frac{\omega}{2z_0^3} e^2 \sin^2 \gamma + \frac{3\omega^2}{8z_0^5} e^4 \sin^4 \gamma, \quad (30)$$

I_2 becomes

$$I_2 = 2\pi\rho_0 r_c^2 \sqrt{1-e^2} \frac{\sqrt{z^2}}{z} \left(\frac{1}{z_0} Q_0 + \frac{1}{2z_0^3} e^2 \sin^2 \gamma Q_1 + \frac{3}{8z_0^5} e^4 \sin^4 \gamma Q_2 \right). \quad (31)$$

Here, Q_n is defined by

$$Q_n \equiv \int_0^{\min(n^2, B_0^2)} \frac{d\omega}{\sqrt{1+\omega}} \tan^{-1} \sqrt{\frac{n^2 - \omega}{1 + \omega}} \omega^n. \quad (32)$$

Their explicit forms are

$$Q_0 = \left[2\sqrt{1+\omega} \tan^{-1} \sqrt{\frac{n^2 - \omega}{1 + \omega}} - 2\sqrt{n^2 - \omega} \right]_0^{\min(n^2, B_0^2)}, \quad (33)$$

$$Q_1 = \left[\frac{1}{9} (12 - 4n^2 - 2\omega) \sqrt{n^2 - \omega} + \frac{2}{3} (\omega - 2) \sqrt{1+\omega} \tan^{-1} \sqrt{\frac{n^2 - \omega}{1 + \omega}} \right]_0^{\min(n^2, B_0^2)}, \quad (34)$$

$$Q_2 = \left[\frac{\sqrt{n^2 - \omega}}{225} (-16(3n^4 - 5n^2 + 15) + 8(5 - 3n^2)\omega - 18\omega^2) - \frac{2}{15} (3\omega^2 - 4\omega + 8) \sqrt{1+\omega} \tan^{-1} \sqrt{\frac{n^2 - \omega}{1 + \omega}} \right]_0^{\min(n^2, B_0^2)}. \quad (35)$$

3. Numerical Calculation of Multiple Images of PG 1115+080

In this section we apply the elliptical lens model with $k = 2$ and $k = 3$ to the multiple quasar of PG 1115+080.

The number of model parameters is 7, namely n , $e \sin \gamma$, r_c , $\rho_0 \sqrt{1 - e^2}$, ϕ , and source positions.

Here, we have introduced the dimensionless parameter κ_0 in place of ρ_0 , defined by

$$\kappa_0 \equiv \frac{8\pi G D_l D_{ls}}{D_s} \rho_0 r_c, \quad (36)$$

which appears as a common factor of the normalized surface mass density. Cosmological parameters, such as z_l , z_s , the Hubble constant and Ω_0 , are assumed to be given. The mass of the lensing galaxy is expressed from equation (6) as

$$M_k = \int \Sigma_k dx dy = \sqrt{\frac{1 - e^2}{1 - e^2 \sin^2 \gamma}} \int K_k dx dy, \quad (37)$$

and calculated to be

$$M_k = 4\pi r_c^3 \rho_0 \sqrt{1 - e^2} \delta_k. \quad (38)$$

Here, δ_k are given by

$$\delta_3 \equiv \frac{1}{2\sqrt{1+n^2}} \int_0^{n^2} \frac{\sqrt{n^2 - \omega}}{\sqrt{1 + \omega}} = \ln(\sqrt{1+n^2} + n) - \frac{n}{\sqrt{1+n^2}} \quad (39)$$

and

$$\delta_2 \equiv \frac{1}{2} \int_0^{n^2} \frac{1}{\sqrt{1+\omega}} \tan^{-1} \sqrt{\frac{n^2 - \omega}{1 + \omega}} d\omega = n - \tan^{-1} n \quad (40)$$

The total number of observed data of Christian et al. is 11, i.e. 4×2 for image positions and 3 for the flux ratios of images (table 2).

We have adopted a new datum for the redshift of the lensing object, $z_l = 0.294$, from Angonin-Willaime et al. (1993). Our fitting procedures were as follows. We obtained parameter values by minimizing the residuals in the source plane, which is defined by

$$f^2 = \sum_{i=1}^4 \left| z_s - z_i + \frac{4GD}{c^2} I^*(z_i) \right|^2. \quad (41)$$

Here z_i is the i -th image position in a complex representation, and we substituted the observed value into it. The image positions are given by the following radial coordinates:

$$l_i = \sqrt{x_i^2 + y_i^2}, \quad \theta_i = \tan^{-1} \frac{y_i}{x_i}. \quad (42)$$

In section 2, we supposed $\phi = 0$. In general, however, the major axis does not coincide with the x -axis (we adopted it parallel to right ascension). Taking the rotation ϕ in the lens surface into consideration, z_i in equation (41) is given by

$$z_i = l_i \cos(\theta_i + \phi) + i l_i \sin(\theta_i + \phi). \quad (43)$$

In order to find the minimum for the f^2 , we have used the downhill-simplex method. We have not incorporated any amplification data in equation (41) because of their unreliability compared with the image positions. We also have not considered the weight in each image, since the error estimate of each image was not given. We calculated the least square function for the $k = 2$ and $k = 3$ models. In order to confirm our calculation, it was checked whether our numerical calculations could reproduce the results of Narasimha et al. if we used the same data as theirs.

We had many parameters, and the fitting parameter region was not necessarily so restricted. Thus, we first fix two parameters, n and $e \sin \gamma$, and then 5 fitting parameters remained to be adjusted. We then changed $e \sin \gamma$ from 0 to 1 by a 0.1 interval. We also chose $n = 5, 10, 20, 30$. For $k=3$ we could fit the parameters in all ranges of n ; the other parameters were insensitive to the n value. On the other hand, for $k=2$ we could fit only for $n = 5$ and 10. For $k=3$, the surface mass density is almost constant for $n \geq 5$, but for $k=2$ it continues to increase for $n \geq 5$. In these procedures, we did not intend to uniquely fit all of the parameters, but to consider the best fitting under the given physically probable parameters, $e \sin \gamma$, n . Using these parameters we also calculated the image positions, amplifications and time delays etc. The results of the best fitting are listed in tables 3 and 4. Table 3 (table 4) is the model for $k = 2$ ($k = 3$). The fitted ϕ 's are very close to each other in spite of the difference in the other parameters. In these tables we have listed the observed image positions in the coordinates, where the x -axis coincides with the major axis of the lenses. The observed image positions and their numerical calculations are depicted in figure 3.

Figure3

From these tables there appears the following image of the lensing object. The core radius ranges over $3-5h^{-1}$ kpc. These values are very large compared with the generally accepted core size. Most of the observations and analyses suggest that the core sizes of elliptical galaxies are few hundred pc (Lauer 1985; Lauer et al. 1991; Bertin et al. 1993). Thus, this large core radius places the single elliptical lens model at a disadvantage. The total mass

is roughly $10^{12} M_{\odot}$ under the assumption $n = 5$ or 10 . The central density ρ_0 roughly equals $10^{-23}h^2$ g cm $^{-3}$.

Therefore, our models exhibit a very weak central concentration compared with the general results of analyses applied to the other lensing events (Kent, Falco 1988; Grogan, Narayan 1996). We have obtained a good fitting for $e \sin \gamma = 0.3\text{-}0.6$. $e \sin \gamma$ (apparent eccentricity) = 0.3 ($e \sin \gamma = 0.6$) is regarded as an E_0 (E_2) galaxy. Thus, our results are compatible with Schechter's observation that the lensing galaxy is round to within 10% (Schechter 1996).

The cut-off radius corresponds to 30-50 Kpc for $n = 10$. These estimates depend on the cosmological parameter Ω_0 . It changes the scale of the parameters through D of equation(13). If we assume $\Omega_0 = 0$ in place of $\Omega_0 = 1$, the core radius, total mass and ρ_0 are estimated to 1.08-, 1.08- and 0.86-times larger than those for $\Omega_0 = 1$, respectively.

As for the image positions, these parameters do not well reproduce the observed values correctly. Especially, as $e \sin \gamma$ becomes larger, it is difficult to fit both A_1 and A_2 with the observations. In their observational data, Christian et al. did not give an error estimate of each image. However, Kristian et al. (1993) observed PG 1115 by HST and determined the image positions at a 5 mas error. These data, however, are not essentially different from the data of Christian et al. By using the data by Kristian et al., we obtained the same parameters as those given in tables 3 and 4 within a 10% difference. We calculated the χ^2 of the image positions from these parameters and data. For example, we obtained the values $\chi^2/\text{DOF} = 1383.48/3$ for $k = 2$, $n = 10$, and $e \sin \gamma = 0.3$, and $\chi^2/\text{DOF} = 572.64/3$ for $k = 3$, $n = 10$, and $e \sin \gamma = 0.5$. These values are extremely large ($\chi^2/\text{DOF} \gg 1$).

As for the image amplifications, the coincidence of the calculated values with the observed ones is not very good. Especially, the calculated magnifications of the B and C components are in reverse order with the observation. Moreover, the predicted value of the undetected image D is too bright.

The predicted time delays in tables 3 and 4 are too short compared with the observation $\Delta t_{BC} = 23\text{-}28$ days (Schechter et al. 1997; Bar-Kana 1997). These results insist that a single transparent lens model can not be applied to this lensing system without any perturbation.

However, we can see the tendency of the parameters according to the change of other parameters for given observational data. From tables 3 and 4, the larger $e \sin \gamma$ becomes, the smaller does the core radius appear. The core radius for $k = 2$ is about 30% smaller than that for $k = 3$. On the contrary, the central density becomes slightly larger, but remains almost unchanged, according to the decreasing core size. The conclusion that the core size becomes smaller with the power law k was also reported by Grogan and Narayan (1996) and Keeton and Kochanek (1997). The reason is as follows. Any lens model predicts almost the same mass within the ring of images. If k

becomes smaller, the mass becomes larger. Therefore, in order to decrease the mass, the core radius must be small with a constant central density. We also remark that the core radius for $k = 2$ decreases by about 10% when n changes from 5 to 10, while that for $k = 3$ almost does not change. Most all researchers have used the expressions for $n = \infty$, because this simplification makes the calculation tractable. However, we left n finite and used approximation (30). The discrepancy between the behaviors of $k = 2$ and 3 may partly come from this difference. In order to check this possibility, we studied the n dependence of the core radius by a spherical symmetric model which is tractable without any approximation. The result is as follows. For $n < 10$, the core radius grows by the order of 1/100 sec totally as n increases, which is negligible in comparison with the present precision of observation. The core radius for $n > 10$ is almost the same as for $n = \infty$. However, we were forced to use $n < 10$, since the core radius is relatively large in our case. The reason why the dependence of core radius on n in our model is larger than the test calculation in the spherical symmetric model may be due to approximation (30).

If the core radius is about several hundred pc, as conventionally adopted, we can take the n order to be several hundred. Thus, n can not play any important role, though ρ_0 decreases as n increases.

Let us compare our result with that by Narasimha et al. for the same $k = 3$ model. For example, some of their best-fit parameters are $n = 20$, $e \sin \gamma = 0.6$, $r_c = 0''.27$, and $\kappa_0 \sqrt{1 - e^2} = 5.946$. Therefore, their model exhibits a much more compact lens model than ours. This discrepancy comes from the difference in the accepted observed data. In their article the lens position was left as a free parameter, since the lensing galaxy had not yet been identified at that time. Therefore, their method of parameter fitting is essentially different from ours. Also, they fit the separations between the images only with observation; therefore, they neglected the relative position of the images and the lens. The data which Narasimha et al. used are $AB = 1.9$, $BC = 2.4$, $CA = 2.0$ and $A_1A_2 = 0.54$ in arcsec. On the other hand, the data of Christian et al. are $AB = 1.8$, $BC = 2.0$, $CA = 2.3$ and $A_1A_2 = 0.49$. BC and CA are reversed in two data. Moreover, their results can not correctly reproduce the observed data. They recorded the separations of images in the unit of the core radius. In matching to the observed image separations, however, their core radius does not converge on one value, and disperses from $0''.26$ to $0''.37$ for each image separation.

Thus, the model parameters are sensitive to the image positions, and especially to the lens position.. To be worse, the error bar of the lens position is still very large, 50 mas (Kristian et al. 1993).

4. Discussion

As we have discussed, the elliptical lens models commonly used give no good fitting, especially concerning the observed image amplifications. Let us consider the possibilities that the observations are biased by something not under consideration so far. Image B is positioned nearer to the lensing galaxy than C (and A₁, A₂). Therefore, B might be brighter than C, but would suffer absorption due to the atmosphere of the lensing galaxy. The old data (Young et al. 1981) suggested this possibility. However, photometry of the QSO components in the new CCD frames (Christian et al. 1987) indicates that the galaxy must be reasonably compact, because there is no reddening of component B relative to C. Therefore, this possibility is unlikely to be true. Another possibility is that the discrepancy may be due to a time delay among the image components. However, this may not also remedy the elliptical lens model, since the predicted time delay (see tables 3 and 4) is too short compared with the observed time variation of amplification (Vanderriest 1986). The elliptical lens model may also raise other troubles. It gives a rather large amplification of undetected image D. However, we can not rule out the possibility that component D is so near to the lens that it suffers from absorption.

However, there is too much evidence to reject the elliptical lens model. Thus, as far as the lensing object is assumed to be isolated, we are attracted to adopt a model that is qualitatively different from the elliptical lens model. A multipole-expansion model is the typical one, which is obtained by expanding the Fermat potential in powers of $1/|\mathbf{x}|$ in equation (11). It should be remarked that the multipole expansion model gives a better fit to the observations than does the elliptical model. Here we quote the main result by the multipole expansion model applied to PG 1115+080 (Kakigi et al. 1995; Fukuyama et al. 1997)

Here, the aspect of the lensing object effectively appears as the multipole components as a whole. We have thus also calculated the multipole components of the elliptical lens model for comparison. Here,

$$m \equiv \frac{1}{\pi} \int d^2x' \kappa(\mathbf{x}') \quad (44)$$

$$q_{ij} \equiv \frac{1}{\pi} \int d^2x' \kappa(\mathbf{x}') (x'_i x'_j - \frac{|\mathbf{x}'|^2}{2} \delta_{ij}) \quad (i, j = 1, 2). \quad (45)$$

In the elliptical lens model, if an image position lies on the ellipse $b = b_0$ in equation (5), it follows from equation (19) that only the mass distribution within $b = b_0$ can contribute to the deflection angle of this image position. Therefore, the multipole moments of the elliptical lens model are estimated by integrating only the $b < b_0$ region in equations (44) and (45). Thus, each image has its own values of multipole moments. The multipole-expansion

model gives a monopole of 3.5×10^{-11} . This value is dimensionless and 1×10^{-10} corresponds to $4.4 \times 10^{11} h^{-1} M_{\odot}$.

Our elliptical lens models give a monopole of $4.4 - 4.7 \times 10^{-11}$ with respect to the outer-most image C and of 2.1×10^{-11} with respect to the inner-most image B, irrespective of the parameters. These values are very near to those of the multipole-expansion model. That is, the mass within the images is the same in the various models. As for the quadrupole moment, that of the elliptical lens model becomes large as $e \sin \gamma$ increases, but there is no difference for the cases $k = 2$ and $k = 3$. Their values are about 1×10^{-23} , and ten-times smaller than that of the multipole-expansion model.

The multipole-expansion model also asserts that the lensing object has a significant dipole moment:

$$d_i \equiv \frac{1}{\pi} \int d^2 x' \kappa(\mathbf{x}') x'_i. \quad (46)$$

An elliptical lens does not have a dipole moment unless the position of the center of mass is shifted from the origin of coordinates. The axis of the dipole moment obtained in the multipole-expansion model (table 6) is nearly parallel to the declination. In order to incorporate the dipole moment in the elliptical lens model, we shifted the origin of coordinates (center of mass) relative to the image positions along the declination and tested whether the data fitting is improved or not. The result was negative.

The discussion so far developed is not advantageous to the single elliptical lens model. A decisive answer, however, requires more precise observations. Recently, the precise spectrum of PG 1115+080 was obtained by Michalitsianos et al. (1996). They revealed that this QSO has a broad absorption line (BAL) of O vi. This means that this QSO has a large-scale outflow gas intrinsic to this QSO. These internal structures of the source must be reflected to that of the image components, and increase the amount of information to be adjusted. Here, as a preliminary step to this new stage, we have listed the result of deformation assuming that the source is spherical. Detailed formulation concerning the shape of the image was developed in Kakigi et al. (1995).

Lastly, we comment on recent studies. A closely connected paper by Keeton and Kochanek (1997) on PG 1115+080 appeared in the Preprint Server three months after our original paper. Firstly, by allowing the parameter freedom to move the lens position from the center of the observed position, they practiced parameter fitting by isolating models. As a result, the χ^2 of the image positions and the amplifications can not be small and the assumed lens position goes beyond the error bar. Their core radius is smaller than ours, since they moved the lens position, but it was still larger than that of an ordinary galaxy. They then applied models corresponding to our $k = 2, 3, 4$ and

de-Vaucouleurs model, all adopting the perturbation by a group of galaxies $14''.5$ apart from the lensing galaxy, and succeeded in obtaining $\chi^2/\text{DOF} < 1$ for all models.

Using the same weight as Keeton and Kochanek, a multipole-expansion model gives $\chi^2/\text{DOF} \simeq 1.5$ (Kakigi 1997, private communication). This value is smaller than those of Schechter et al. (1997), whose models take the effect of nearby galaxies into consideration by shear. Therefore, the fact that an isolated transparent lens model gives no good fitting does not necessarily lead us to conclude the presence of a perturbation due to nearby galaxies.

Thus, χ^2/DOF of the image positions and the amplifications can be equal or less than unit in several lens models. For determining models, a χ^2 fitting is not sufficient. Both quantitative and qualitative arguments from various viewpoints complement this deficit. For that purpose, analytical surveys of lensing models like those developed in section two seem to become more important.

This paper is summarized as follows. We applied the elliptical lens model with softened power-law behaviors of $k = 2$ and $k = 3$ to the multiple QSO PG 1115+080. Using the obtained fitting parameters, we calculated other observables. Firstly, the elliptical lens models do not well produce the image positions. Secondly, the image amplifications do not well coincide with the observed values. Finally, we obtained a relatively large core radius. For the above reasons, we are forced to conclude that this model with $k = 2$ and $k = 3$ can not be consistent with the observations. As an alternative model, if we accept a non-transparent model, the lens may have an asymmetric mass distribution with a non zero dipole moment, as was suggested by the multipole-expansion model. It is very natural to consider that this dipole moment reflects the presence of the nearby group of galaxies (Young et al. 1981). However, the direction of the dipole moment deviates from that of the nearby group by 100° . We have no clear explanation for this fact.

In any case, we have not derived any definite picture of the lensing galaxy due to gravitational lensing. We are enthusiastically waiting for more precise data, such as spectroscopy profiles of the individual image components (Michalitsianos, Oliverson 1995), their time variations and the image substructures etc.

We are grateful to a referee who made very constructive and useful comments to us.

References

Angonin-Willaime M.-C., Hammer F., Rigaut F. 1993, in Proc. 31st Liège Int. Astrophys. Colloq., Gravitational Lenses in the Universe, ed J.Surdej, D.Fraipont-Caro, E.Gosset, S.Refsdal, M.Remy (Institut d'Astrophysique, Liège) p85

Bahcall N.A., Lubin L.M. 1994, ApJ 426, 513

Bar-Kana R. 1997, ApJ 489, 21

Bertin G., Pignatelli E., Saglia R.P. 1993, A&A 271, 381

Binney J., Tremaine S. 1987, Galactic Dynamics (Princeton University Press, Princeton) ch1

Bourassa R.R., Kantowski R., Norton T.D. 1973, ApJ 185, 747

Bourassa R.R., Kantowski R. 1975, ApJ 195, 13

Christian C.A., Crabtree D., Waddell P. 1987, ApJ 312, 45

Fukuyama T., Kakigi Y., Okamura T. 1997, Int. J. Mod. Phys. D 6, 425

Grogin N.A., Narayan R. 1996, ApJ 464, 92

Kakigi Y., Okamura T., Fukuyama T. 1995, Int. J. Mod. Phys. D 4, 685

Kassiola A., Kovner I. 1993, ApJ 417, 450

Keeton C.R., Kochanek C.S. 1997, ApJ 487, 42

Kent S.M., Falco E.E. 1988, AJ 96, 1570

Kormann R., Schneider P., Bartelmann M. 1994, A&A 284, 285

Kristian J., Groth E.J., Shaya E.J., Schneider D.P., Holtzman J.A., Baum W.A., Campbell B., Code A. et al. 1993, AJ 106, 1330

Lauer T.R. 1985, ApJ 292, 104

Lauer T.R., Faber S.M., Holtzman J.A., Baum W.A., Currie D.G., Ewald S.P., Groth E.J., Hester J.J. et al. 1991, ApJ 369, L41

Michalitsianos A.G., Oliverson R.J. 1995, ApJ 439, 599

Michalitsianos A.G., Oliverson R.J., Nichols J. 1996, ApJ 461, 593

Miralda-Escudé J. 1993, ApJ 403, 497

Narasimha D., Subramanian K., Chitre S.M. 1982, MNRAS 200, 941

Schechter P.L. 1996, in Proc. Astrophysical Applications of Gravitational Lensing, ed C.S.Kochanek, J.N.Hewitt (Kluwer, Dordrecht) p263

Schechter P.L., Bailyn C.D., Barr R., Barvainis R., Becker C.M., Bernstein G.M., Blakeslee J.P., Bus S.J. et al. 1997, ApJ 475, L85

Schramm T. 1990, A&A 231, 19

Vanderriest C., Wléric G., Lelièvre G., Schneider J., Sol H., Horville D., Renard L., Servan B. 1986, A&A 159, L5

Yoshida H., Omote M. 1988, Prog. Theor. Phys. 79, 1095

Young P., Deverill R.S., Gunn J.E., Westphal J.A., Kristian J. 1981, ApJ 244, 723

Figure Captions

Fig. 1. Two Euler angles γ and ϕ in a spheroid. ϕ is the rotation angle between the x -axis and the major axis of the lens in the lens plane.

Fig. 2. Schematic diagram of the gravitational-lens geometry. The solid line shows the real light path.

Fig. 3. Observed image positions (circles) and their numerical calculations (squares). The solid lines are the caustics and dashed lines are the critical lines. Here, the adopted parameters are those of $k=3$, $n=10$ and $e \sin \gamma = 0.5$ in table 4.

Table 1. Parameters of lensing object.

Parameters	Symbol
Eccentricity	e
Inclination	$\sin \gamma$
Core radius	r_c
Cut-off radius	$n \cdot r_c$
Source position	(x_s, y_s)
Normalized central density	κ_0
Rotation angle in lens plane	ϕ

* e and $\sin \gamma$ appear only in the combined form of $e \sin \gamma$.

Table 2. Observed image positions and their amplifications relative to C component in PG 1115+080.

Image	x_i	y_i	μ/μ_C
A ₁	$-0''.94$	$-0''.73$	3.22
A ₂	$-1''.11$	$-0''.27$	2.49
B	$0''.72$	$-0''.60$	0.64
C	$0''.33$	$1''.35$	1.00

Table 3. Numerical calculations of the image positions for the $k=2$ case.

n	5		
$e \sin \gamma$	0.3	0.4	0.5
$r_c (h^{-1}\text{kpc})$	1''.86 (5.16)	1''.31 (3.64)	0''.97 (2.69)
$\kappa_0 \sqrt{1 - e^2} (h^2 \text{ g cm}^{-3})$	0.77 (2.17×10^{-23})	0.82 (3.28×10^{-23})	0.88 (4.76×10^{-23})
Total mass	$1.99 \times 10^{12} M_\odot h^{-1}$	$1.06 \times 10^{12} M_\odot h^{-1}$	$6.19 \times 10^{11} M_\odot h^{-1}$
Source position	(0''.014, -0''.020)	(0''.025, -0''.036)	(0''.039, -0''.055)
Image positions (Time delay lagging behind C in day h^{-1})			
A ₁ (fitting)	(0''.52, 1''.08)(1.5)	(0''.54, 1''.06)(2.7)	(0''.54, 1''.05)(4.1)
A ₁ (observed)	(0''.59, 1''.03)	(0''.58, 1''.04)	(0''.57, 1''.04)
A ₂ (fitting)	(0''.94, 0''.64)(1.5)	(0''.96, 0''.62)(2.8)	(0''.99, 0''.58)(4.2)
A ₂ (observed)	(0''.92, 0''.67)	(0''.92, 0''.68)	(0''.91, 0''.69)
B(fitting)	(-0''.88, 0''.32)(2.2)	(-0''.88, 0''.31)(4.3)	(-0''.89, 0''.29)(6.5)
B(observed)	(-0''.89, 0''.28)	(-0''.90, 0''.27)	(-0''.90, 0''.26)
C(fitting)	(0''.23, -1''.37)	(0''.26, -1''.36)	(0''.28, -1''.36)
C(observed)	(0''.21, -1''.37)	(0''.22, -1''.37)	(0''.24, -1''.37)
D(fitting)	(-0''.20, 0''.27)	(-0''.20, 0''.09)	(-0''.18, 0''.08)
n	10		
$e \sin \gamma$	0.3	0.4	0.5
$r_c (h^{-1}\text{kpc})$	1''.69 (4.70)	1''.23 (3.41)	0''.88 (2.44)
$\kappa_0 \sqrt{1 - e^2} (h^2 \text{ g cm}^{-3})$	0.73 (2.26×10^{-23})	0.77 (3.28×10^{-23})	0.84 (5.00×10^{-23})
Total mass	$3.67 \times 10^{12} M_\odot h^{-1}$	$2.05 \times 10^{12} M_\odot h^{-1}$	$1.15 \times 10^{12} M_\odot h^{-1}$
Source position	(0''.014, -0''.021)	(0''.025, -0''.035)	(0''.040, -0''.054)
Image positions (Time delay lagging behind C in day h^{-1})			
A ₁ (fitting)	(0''.56, 1''.04)(1.5)	(0''.52, 1''.07)(2.7)	(0''.54, 1''.05)(4.1)
A ₁ (observed)	(0''.58, 1''.04)	(0''.58, 1''.04)	(0''.57, 1''.05)
A ₂ (fitting)	(0''.92, 0''.67)(1.6)	(0''.92, 0''.61)(2.8)	(0''.99, 0''.57)(4.2)
A ₂ (observed)	(0''.91, 0''.69)	(0''.92, 0''.68)	(0''.91, 0''.70)
B(fitting)	(-0''.90, 0''.31)(2.4)	(-0''.89, 0''.30)(4.3)	(-0''.89, 0''.29)(6.6)
B(observed)	(-0''.90, 0''.27)	(-0''.90, 0''.27)	(-0''.90, 0''.26)
C(fitting)	(0''.23, -1''.35)	(0''.26, -1''.36)	(0''.28, -1''.36)
C(observed)	(0''.23, -1''.37)	(0''.23, -1''.37)	(0''.24, -1''.37)
D(fitting)	(-0''.30, 0''.36)	(-0''.24, 0''.29)	(-0''.17, 0''.22)

* The upper part is the adopted values of the parameters, and the lower part is the corresponding theoretical values and time delay in units of days h^{-1} . We have also listed the observed values for a comparison. The parenthesized values in lines of r_c and $\kappa_0 \sqrt{1 - e^2}$ are the physical core size in units of $h^{-1}\text{kpc}$ and the central density, $\rho_0 \sqrt{1 - e^2}$ in units of $h^2 \text{ g cm}^{-3}$, respectively. Here, we assume $\Omega_0 = 1$, $H_0 = 100h \text{ km s}^{-1} \text{ Mpc}$, $z_l = 0.3$ and $z_s = 1.72$.

Table 4. The same calculations as in table 3 for the $k=3$ case.

n	5		
$e \sin \gamma$	0.4	0.5	0.6
$r_c (h^{-1}\text{kpc})$	1''.90 (5.27)	1''.48 (4.11)	1''.19 (3.30)
$\kappa_0 \sqrt{1-e^2} (h^2 \text{ g cm}^{-3})$	1.13 (3.12×10^{-23})	1.19 (4.21×10^{-23})	1.28 (5.64×10^{-23})
Total mass	$1.12 \times 10^{12} M_\odot h^{-1}$	$7.17 \times 10^{11} M_\odot h^{-1}$	$4.99 \times 10^{11} M_\odot h^{-1}$
Source position	(0''.024, -0''.037)	(0''.038, -0''.058)	(0''.057, -0''.085)
Image positions (Time delay lagging behind C in day h^{-1})			
A ₁ (fitting)	(0''.51, 1''.08)(2.8)	(0''.53, 1''.06)(4.3)	(0''.53, 1''.05)(6.3)
A ₁ (observed)	(0''.59, 1''.03)	(0''.58, 1''.04)	(0''.57, 1''.04)
A ₂ (fitting)	(0''.95, 0''.63)(2.9)	(0''.97, 0''.61)(4.4)	(1''.00, 0''.57)(6.4)
A ₂ (observed)	(0''.92, 0''.67)	(0''.92, 0''.68)	(0''.91, 0''.69)
B(fitting)	(-0''.88, 0''.31)(4.2)	(-0''.89, 0''.30)(6.6)	(-0''.89, 0''.28)(9.7)
B(observed)	(-0''.89, 0''.28)	(-0''.90, 0''.27)	(-0''.90, 0''.26)
C(fitting)	(0''.23, -1''.37)	(0''.24, -1''.37)	(0''.26, -1''.37)
C(observed)	(0''.21, -1''.37)	(0''.22, -1''.37)	(0''.24, -1''.37)
D(fitting)	(-0''.17, 0''.15)	(-0''.16, 0''.13)	(-0''.15, 0''.12)
n	10		
$e \sin \gamma$	0.4	0.5	0.6
$r_c (h^{-1}\text{kpc})$	1''.88 (5.22)	1''.46 (4.05)	1''.16 (3.22)
$\kappa_0 \sqrt{1-e^2} (h^2 \text{ g cm}^{-3})$	1.11 (3.10×10^{-23})	1.18 (4.24×10^{-23})	1.27 (5.74×10^{-23})
Total mass	$1.62 \times 10^{12} M_\odot h^{-1}$	$1.04 \times 10^{12} M_\odot h^{-1}$	$7.07 \times 10^{11} M_\odot h^{-1}$
Source position	(0''.024, -0''.037)	(0''.039, -0''.058)	(0''.057, -0''.084)
Image positions (Time delay lagging behind C in day h^{-1})			
A ₁ (fitting)	(0''.51, 1''.08)(2.7)	(0''.53, 1''.06)(4.3)	(0''.53, 1''.05)(6.2)
A ₁ (observed)	(0''.59, 1''.03)	(0''.58, 1''.04)	(0''.57, 1''.05)
A ₂ (fitting)	(0''.96, 0''.62)(2.8)	(0''.97, 0''.61)(4.4)	(1''.00, 0''.57)(6.4)
A ₂ (observed)	(0''.93, 0''.67)	(0''.92, 0''.68)	(0''.91, 0''.69)
B(fitting)	(-0''.89, 0''.31)(4.1)	(-0''.89, 0''.30)(6.7)	(-0''.89, 0''.28)(9.7)
B(observed)	(-0''.90, 0''.28)	(-0''.90, 0''.27)	(-0''.90, 0''.26)
C(fitting)	(0''.24, -1''.37)	(0''.25, -1''.37)	(0''.26, -1''.37)
C(observed)	(0''.21, -1''.37)	(0''.22, -1''.37)	(0''.24, -1''.37)
D(fitting)	(-0''.17, 0''.15)	(-0''.16, 0''.13)	(-0''.15, 0''.12)

Table 5. Numerical calculations of image amplifications.

k	2			3		
$e \sin \gamma$	0.3	0.4	0.5	0.4	0.5	0.6
n	5	10	5	10	5	10
A ₁ /C	4.45	6.15	3.92	3.65	3.03	2.91
A ₂ /C	4.45	4.20	3.81	3.61	2.91	2.74
B/C	2.31	1.95	1.91	1.82	1.54	1.44
D/C	1.90	2.67	1.08	1.67	0.72	0.85

Table 6. Numerical calculations by the multipole-expansion model.

m	3.50×10^{-11}		
$ d $	$3.77 \times 10^{-17} (7.80 \times 10^{-19}, 3.77 \times 10^{-17})$		
$ q $	$1.07 \times 10^{-22} (-6.93 \times 10^{-23}, 8.10 \times 10^{-23})$		
Image positions			
Amplification relative to C			
Time delay lagging behind C in day h^{-1}			
A ₁	(-0.9383'', -0.7317'')	3.113	9.757
A ₂	(-1.110'', -0.2748'')	2.892	11.448
B	(0.7205'', -0.6004'')	0.7467	19.407
C	(0.3294'', 1.350'')	1.000	0.000
D	(0.5915'', -0.4450'')	0.1780	19.225
E	(-0.4494'', 0.08641'')	0.005871	3.076

* Multipole components are defined by equations (44)-(46). The bracket in lines of $|d|$ and $|q|$ means (d_1, d_2) and (q_{11}, q_{12})

components, respectively. (From Fukuyama et al. 1997)

Table 7. Calculated image eccentricity and angle between the major axis of the image and the x -axis for the $k=2$ case.

$e \sin \gamma$		0.3		0.4		0.5	
n		5	10	5	10	5	10
A ₁	Eccentricity(Axis ratio)	0.9958(0.092)	0.9981(0.062)	0.9949(0.101)	0.9944(0.106)	0.9921(0.125)	0.9917(0.129)
Angle		$-30^\circ.2$	$-32^\circ.7$	$-30^\circ.7$	$-29^\circ.6$	$-30^\circ.2$	$-30^\circ.2$
A ₂	Eccentricity(Axis ratio)	0.9944(0.106)	0.9952(0.098)	0.9931(0.117)	0.9925(0.122)	0.9890(0.148)	0.9885(0.151)
Angle		$-60^\circ.6$	$-58^\circ.5$	$-61^\circ.0$	$-61^\circ.4$	$-62^\circ.3$	$-62^\circ.7$
B	Eccentricity(Axis ratio)	0.8378(0.546)	0.8662(0.500)	0.8193(0.573)	0.8389(0.544)	0.7995(0.601)	0.8175(0.576)
Angle		$74^\circ.5$	$74^\circ.8$	$74^\circ.5$	$75^\circ.1$	$75^\circ.3$	$75^\circ.2$
C	Eccentricity(Axis ratio)	0.9756(0.220)	0.9787(0.205)	0.9735(0.229)	0.9726(0.233)	0.9707(0.240)	0.9693(0.246)
Angle		$10^\circ.9$	$11^\circ.0$	$12^\circ.2$	$12^\circ.3$	$13^\circ.1$	$13^\circ.2$

Table 8. The same calculations as in table 7 for the $k=3$ case.

$e \sin \gamma$		0.4		0.5		0.6	
n		5	10	5	10	5	10
A ₁	Eccentric- ity(Axis ratio)	0.9952(0.098)	0.9952(0.098)	0.9948(0.102)	0.9948(0.102)	0.9934(0.115)	0.9933(0.116)
Angle		$-28^\circ.7$	$-28^\circ.6$	$-28^\circ.9$	$-28^\circ.9$	$-27^\circ.6$	$-27^\circ.6$
A ₂	Eccentric- ity(Axis ratio)	0.9937(0.112)	0.9933(0.115)	0.9925(0.122)	0.9922(0.124)	0.9890(0.148)	0.9892(0.146)
Angle		$-60^\circ.5$	$-61^\circ.1$	$-60^\circ.6$	$-60^\circ.6$	$-61^\circ.7$	$-61^\circ.7$
B	Eccentric- ity(Axis ratio)	0.8025(0.597)	0.8202(0.572)	0.7860(0.618)	0.7854(0.619)	0.7129(0.701)	0.7209(0.693)
Angle		$74^\circ.6$	$74^\circ.7$	$74^\circ.6$	$74^\circ.5$	$74^\circ.8$	$74^\circ.8$
C	Eccentric- ity(Axis ratio)	0.9735(0.228)	0.9739(0.227)	0.9704(0.241)	0.9704(0.242)	0.9659(0.259)	0.9656(0.260)
Angle		$10^\circ.4$	$10^\circ.9$	$10^\circ.4$	$10^\circ.8$	$10^\circ.6$	$10^\circ.6$

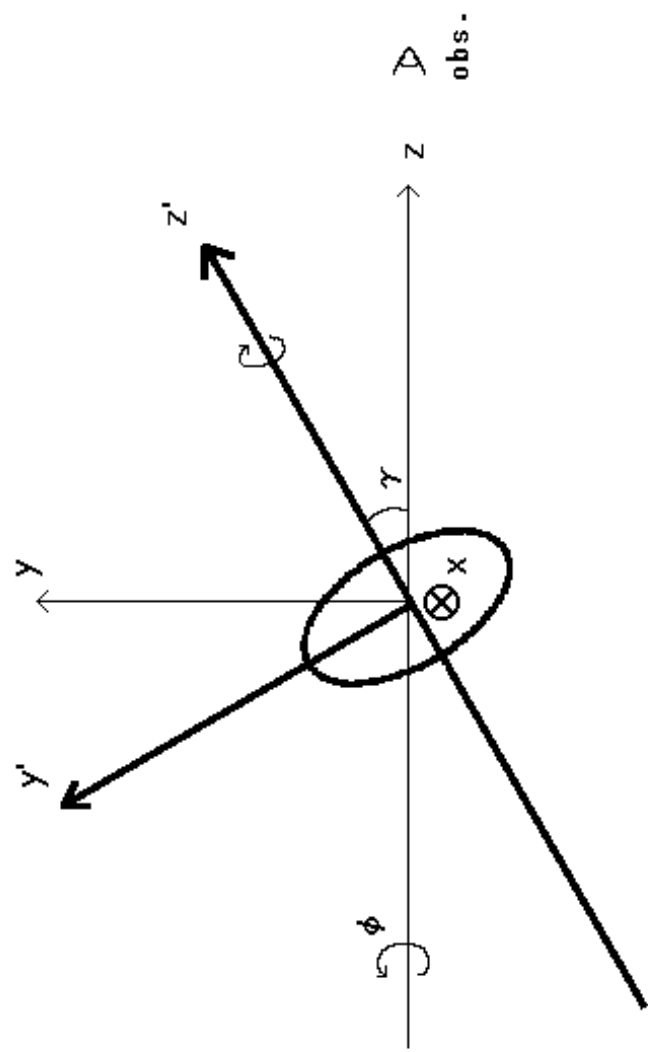
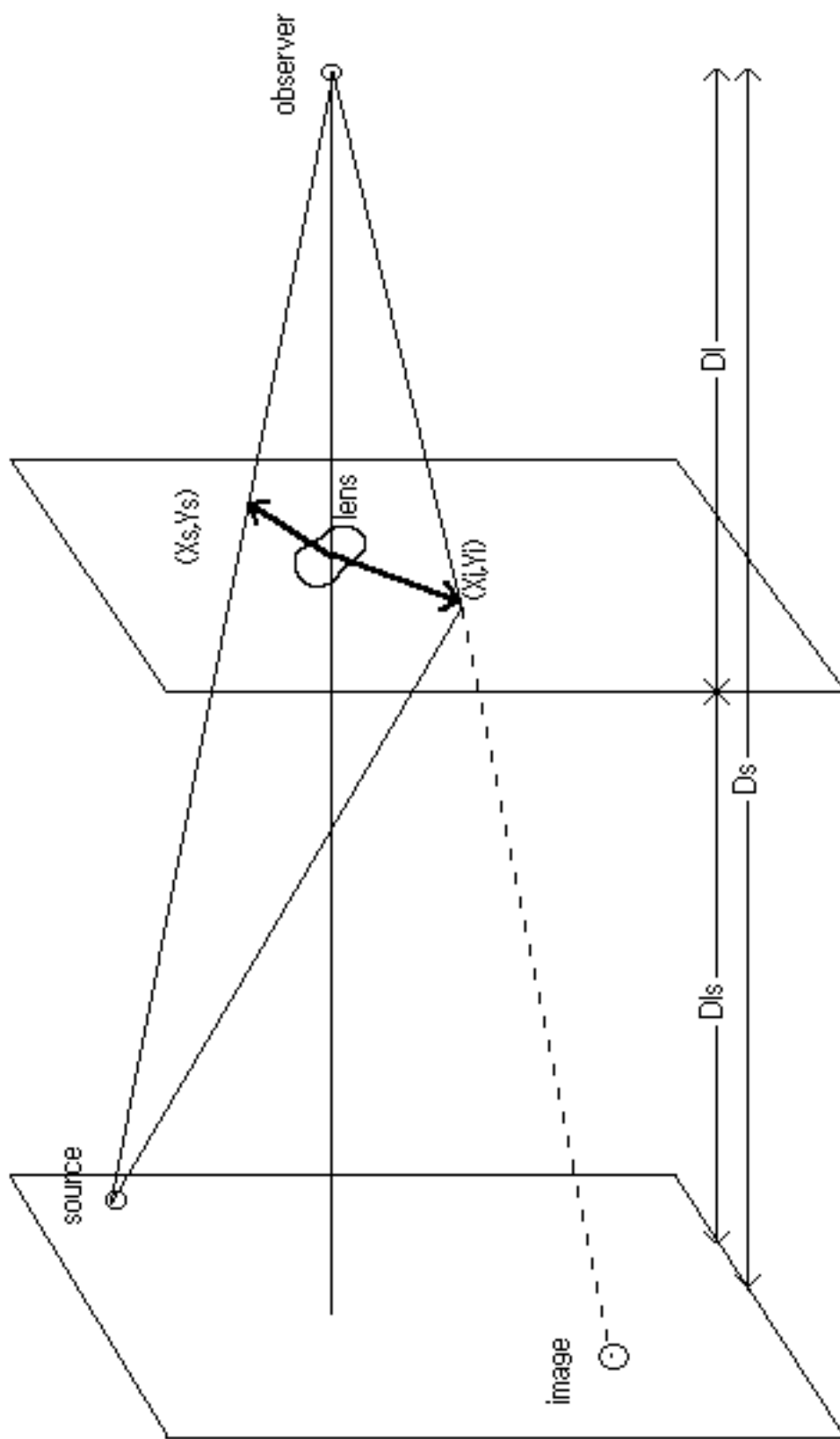


Fig. 1

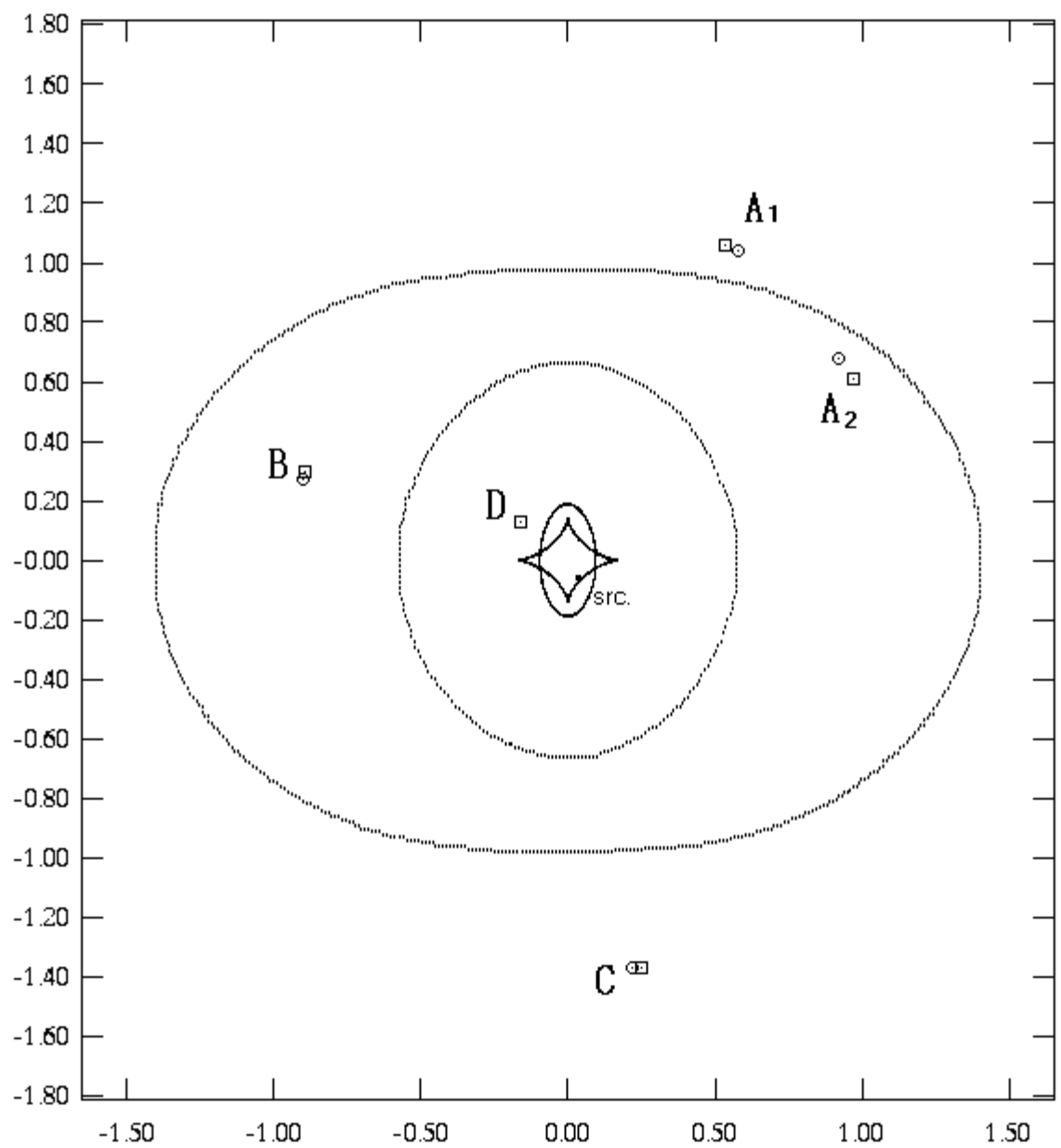
K. Asano and T. Fukuyama

K.Asano and T.Fukuyama

Fig.2



Y



X

Fig.3

K.Asano and T.Fukuyama